



CrossMark
click for updates

Cite this: *Chem. Sci.*, 2015, 6, 4599

Bidirectional photoswitching of magnetic properties at room temperature: ligand-driven light-induced valence tautomerism†

Alexander Witt, Frank W. Heinemann and Marat M. Khusniyarov*

Valence tautomeric (VT) metal complexes are highly promising bistable molecular compounds for applications as molecular switches in molecular electronics and spintronics. Although VT species can be switched with light, the photoswitching in all reported systems requires very low temperatures (usually below 20 K) because photoinduced states are highly unstable at room temperature. The thermal instability hinders any practical application of these complexes in genuine devices. In this report, for the first time we demonstrate photoswitching of VT species and associated magnetic properties at room temperature. The bidirectional photoswitching in solution is due to *cis-trans* photoisomerizable 4-styrylpyridine ligands deliberately integrated into cobalt dioxolene molecular complexes. The novel type of photoswitching has been coined Ligand-Driven Light-Induced Valence Tautomerism (LD-LIVT). The photoconversion of VT states of 28% has been achieved in solution at room temperature. The photoinduced states show extraordinary thermal stability for hours at room temperature, as compared to common nanoseconds reported previously. The switching proceeds at molecular level with the effective photoswitching rate of 3×10^{13} molecules per s under our conditions. Consequently, this work may open new horizons in applications of molecular switches based on VT metal complexes in molecular devices functioning at room temperature.

Received 13th January 2015

Accepted 22nd May 2015

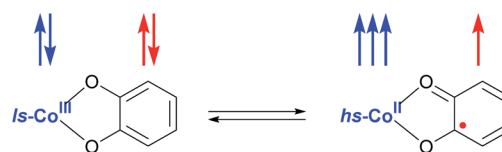
DOI: 10.1039/c5sc00130g

www.rsc.org/chemicalscience

Introduction

Valence tautomeric (VT) metal complexes are well known systems showing molecular bistability.^{1,2} The close energies of metal- and ligand-based redox-active orbitals allow a reversible intramolecular electron transfer to occur, which gives rise to distinctly different electronic states (redox isomers). Particularly interesting are VT cobalt dioxolenes because intramolecular electron transfer is accompanied by a spin state change at the cobalt center resulting in reversible switching between diamagnetic low-spin (ls) cobalt(III) ($S = 0$) and paramagnetic high-spin (hs) cobalt(II) ($S = 3/2$) ions. Greatly differing magnetic properties of the two states and the opportunity to switch reversibly between them by external stimuli render VT cobalt complexes highly attractive for applications as molecular switches, sensors and molecule-based memory units.^{3–6}

The switching in VT metal complexes can be triggered by temperature, pressure, magnetic field, soft X-rays or by light.⁷



Most of the research in the field is dedicated to the development of thermally switchable VT species. However, switching with light is much more attractive for prospective applications due to high speed of addressing, superior resolution, and high selectivity. It is known that photoswitching in VT metal complexes can be achieved by irradiation into appropriate charge transfer (CT) absorption bands.⁸ However, the lifetime of such photoinduced metastable states is in the order of nanoseconds at room temperature (RT). The metastable states can be stabilized by cooling which allows the photoswitching to be performed only at very low temperatures, usually below 20 K.^{9–12} Shultz *et al.* were able to stabilize photoinduced states at higher temperatures up to 90 K using crystal lattice effects.^{13,14} However, the photoswitching becomes impossible at molecular level in such a case. Thus, all previously reported VT photoswitches operate only at very low temperatures, which results in serious limitations for their use in molecular devices.

Friedrich-Alexander-University of Erlangen-Nuremberg, Department of Chemistry and Pharmacy, Egerlandstr. 1, 91058 Erlangen, Germany. E-mail: marat.khusniyarov@fau.de; Fax: +49 9131 8527367; Tel: +49 9131 8527464

† Electronic supplementary information (ESI) available: Derivation of the non-linear regression fitting functions, crystallographic details, magnetization and electrochemical data, EPR and electronic absorption spectra. CCDC 1015850–1015852 and 1058866. For ESI and crystallographic data in CIF or other electronic format see DOI: 10.1039/c5sc00130g



Nonetheless, a photoinduced state might be stabilized by introducing photoisomerizable ligands into VT systems¹⁵ in such a way that a ligand-based photoreaction affects the energy of redox-active orbitals and thus triggers intramolecular electron transfer. The stability of such photoinduced state is dictated by the stability of the photoisomer of the ligand which can exceed years at RT.¹⁶ The very first step in this direction has been attempted recently by Frank *et al.*¹⁷ Although their spirooxazine-derived ligand maintained photoactivity within a VT cobalt complex, no solid evidence for the photoswitching of VT states at RT has been provided. Thus, VT metal complexes that can be switched with light at RT remained unknown to date.

Our group works on stabilization of photoinduced states in VT and spin-crossover metal complexes by integration of photoisomerizable ligands into bistable species.^{18–20} Very recently, we have developed a VT cobalt dioxolene system featuring two photoactive *trans*-4-phenylazopyridine ligands and introduced a new concept for switching VT states called “Coordination-Induced Valence Tautomerism” (CIVT).²⁰ Unfortunately, low thermal stability of photogenerated *cis*-4-phenylazopyridine precluded a detailed examination of photoswitching in this system. To improve photophysical properties of the system we decided to substitute 4-phenylazopyridine with 4-styrylpyridine (4-styryl) ligands that show high thermal stability of both *cis*- and *trans*-isomers.²¹

Here, we report two VT cobalt complexes *trans*-6 and *cis*-6 containing photoactive *trans*-4-styryl and *cis*-4-styryl ligands, respectively (Scheme 1). Their molecular and electronic structures are thoroughly investigated by variable-temperature X-ray crystallography, magnetic susceptibility measurements, NMR, EPR and electronic absorption spectroscopy, electrochemistry and titration experiments. For the first time, the electronic states of VT metal complexes are switched with light at room temperature. Consequently, the switching of VT states allows to

control magnetic properties with light at ambient temperatures. This opens new horizons for application of molecular switches based on VT metal complexes in functioning molecular devices.

Experimental section

Materials

All starting materials and solvents were used as received without further purification unless otherwise noted. Pure anhydrous solvents, required for work under inert atmosphere, were collected from a solid state solvent purification system (Glass Contour System, Irvine, CA) and stored over activated molecular sieves.

Syntheses

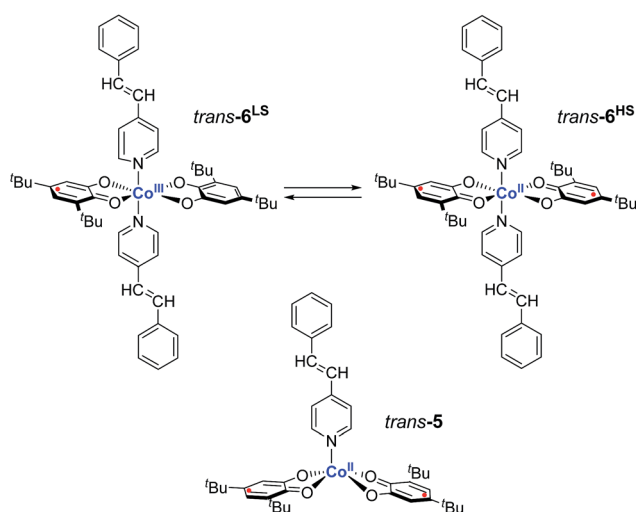
Precursor cobalt tetramer was obtained as a benzene solvate $[\text{Co}(\text{tbdiox})_2]_4 \cdot (\text{C}_6\text{H}_6)_{2.75}$ by a synthetic procedure described by Pierpont *et al.*²² *trans*-4-Styrylpyridine (*trans*-4-styryl) was prepared according to a method described by Chiang and Hartung.²³ *cis*-4-Styrylpyridine (*cis*-4-styryl) was obtained in a Wittig reaction as reported by Williams *et al.*²¹

$[\text{Co}(\text{tbdiox})_2(\text{trans-4-styryl})_2]$ (*trans*-6) was prepared according to a common procedure for bis(*o*-dioxolene) cobalt complexes:¹ under inert atmosphere, *trans*-4-styrylpyridine (200 mg, 1.10 mmol) dissolved in toluene (10 mL) was added dropwise to $[\text{Co}(\text{tbdiox})_2]_4 \cdot (\text{C}_6\text{H}_6)_{2.75}$ (300 mg, 0.14 mmol) dissolved in hot toluene (50 mL, 80 °C). The reaction mixture was stirred overnight at 80 °C and then stored at –35 °C for 3 days before a grey-green precipitate was collected and dried *in vacuo* (274 mg, yield: 58%). Elemental analysis calcd (%) for $\text{C}_{54}\text{H}_{62}\text{CoN}_2\text{O}_4$: C 75.24, H 7.25, N 3.25; found: C 74.99, H 7.24, N 3.32.

$[\text{Co}(\text{tbdiox})_2(\text{cis-4-styryl})_2]$ (*cis*-6) was obtained following a similar synthetic protocol: under inert atmosphere, *cis*-4-styrylpyridine (295 mg, 1.63 mmol) was added to a hot toluene solution (70 mL, 80 °C) of $[\text{Co}(\text{tbdiox})_2]_4 \cdot (\text{C}_6\text{H}_6)_{2.75}$ (448 mg, 0.20 mmol). The reaction mixture was stirred for 2 days at 80 °C and then stored at –35 °C for several days before a black crystalline precipitate was collected and dried *in vacuo* (503 mg, yield: 73%). Elemental analysis calcd (%) for $\text{C}_{54}\text{H}_{62}\text{CoN}_2\text{O}_4$: C 75.24, H 7.25, N 3.25; found: C 75.83, H 7.13, N 3.36.

Instrumentation and physical measurements

Elemental analyses were carried out with a EURO EA analyser from Euro Vector. Magnetic susceptibility data on solid samples were collected using a Quantum Design MPMS-XL SQUID magnetometer. The data were obtained for microcrystalline samples restrained within a polycarbonate gel capsule. DC susceptibility data were collected in the temperature range 2–400 K at applied magnetic field of 1 T. The program *JulX* was used for the simulation and analysis of magnetic data.²⁴ Electrochemical measurements were performed under nitrogen atmosphere at RT using a standard three-electrode setup with glassy carbon working electrode and platinum rods as counter and reference electrodes. The potentiostat was a μ Autolab Type-III. Analyte solutions were prepared in CH_2Cl_2 containing 0.1 M $n\text{-Bu}_4\text{NPF}_6$ as supporting electrolyte. All potentials are referenced



Scheme 1 Cobalt dioxolene complexes *trans*-5 and *trans*-6 with their respective electronic structures: $[\text{ls-Co}^{\text{III}}(\text{Cat})(\text{SQ})(\text{trans-4-styryl})_2]$ (*trans*-6^{LS}), $[\text{hs-Co}^{\text{II}}(\text{SQ})_2(\text{trans-4-styryl})_2]$ (*trans*-6^{HS}), and $[\text{hs-Co}^{\text{II}}(\text{SQ})_2(\text{trans-4-styryl})_2]$ (*trans*-5). Molecular and electronic structures of *cis*-5 and *cis*-6 are similar except of *trans*-4-styryl substituted by *cis*-4-styryl.



to the $\text{Fc}^{+/0}$ redox couple measured after adding ferrocene to the analyte solution. EPR spectra were recorded on a Jeol CW spectrometer JES-FA200 equipped with an X-band Gunn diode oscillator bridge and a cylindrical mode cavity. Simulations were performed using the program W95EPR written by F. Neese.²⁵ Irradiation experiments were conducted *in situ* through a quartz window in the cavity. NMR spectra of *trans*-6 in solution were recorded in rotating 5 mm o.d. tubes with Jeol JNM-LA 400 FT NMR spectrometer and processed with Delta V4.0 software provided by Jeol Ltd. NMR spectra of *cis*-6 in solution were obtained without rotating, in 5 mm o.d. tubes on a Bruker Avance DRX 400 WB spectrometer and processed with TopSpin 1.3 software. Magnetic susceptibility in solutions were determined by the Evans NMR method.²⁶ During the variable temperature and titration experiments the outer tube (standard 5 mm o.d. NMR tube with a PTFE spindle valve) contained a reference solvent mixture $\text{C}_7\text{H}_8/\text{C}_7\text{D}_8/\text{TMS}$ (10/2/1), while the inner tube (capillary tube with 1.5 mm diameter sealed with inert wax) contained the paramagnetic complex in the same solvent mixture. The irradiation experiments were performed using a rotating 5 mm o.d. quartz NMR tube with a PTFE spindle valve with the complex solution in the outer tube and the reference solvent mixture in the inner capillary tube. Electronic absorption spectra were recorded with a Shimadzu UV 3600 spectrophotometer. The samples were prepared under anaerobic conditions and sealed in QS Quartz Suprasil cells (10 mm light path) with PTFE spindle valves. Variable-temperature spectra were recorded with an Analytik Jena SPECORD S600 spectrophotometer. The samples were prepared under anaerobic conditions and measurements were conducted inside a glove box using QS Quartz Suprasil cells (10 mm light path). The solutions were continuously stirred with a magnet bar and

the temperature inside the cells was monitored. An LOT-Oriel Xe(OF) arc lamp (1 kW) equipped with an Omni- λ 300 monochromator was used as a wavelength-variable light source in all irradiation experiments except the *in situ* irradiation followed by EPR spectroscopy. For the latter, an LOT-Oriel Xe(OF) arc lamp (150 W) equipped with an Andover bandpass filter (CWL: 322.9 nm, T_{max} : 28.0%, FWHM: 10.6 nm) were employed.

X-ray crystallographic data collection and structure refinement

Suitable crystals were embedded in protective perfluoropolyalkyl ether oil and transferred to the cold nitrogen gas stream of the diffractometer. Intensity data for *trans*-6 were collected at 120, 295 and 305 K, and for *cis*-6 at 100 K on a Bruker Kappa Smart APEX2 (Mo K_α radiation, $\lambda = 0.71073$ Å, graphite monochromator). Data were corrected for Lorentz and polarization effects; semi empirical absorption corrections were applied on the basis of multiple scans using SADABS.²⁷ The structures were solved by direct methods and refined by full-matrix least squares procedures on F^2 using SHELXTL NT 6.12.²⁸ All non-hydrogen atoms were refined with anisotropic displacement parameters. Hydrogen atoms were placed in position of optimized geometry and their isotropic displacement parameters were tied to those of their corresponding carrier atoms by a factor of 1.2 or 1.5. SIMU and ISOR restraints were applied in the refinement of the disorder. The crystallographic data, data collection and structure refinement details are summarized in Table 1 (ESI†).

At temperatures of 120 K and 295 K *trans*-6 was situated on a general position of space group $P\bar{1}$. While at 120 K the molecule was well ordered, disorder was observed at higher temperatures. At 295 K the two pyridyl ligands were subjected to orientational

Table 1 Crystallographic data, data collection and structure refinement details for *trans*-6 and *cis*-6

	<i>trans</i> -6	<i>trans</i> -6	<i>trans</i> -6	<i>cis</i> -6·4(C ₇ H ₈)
Temperature, K	120	295	305	100
Chemical formula	C ₅₄ H ₆₂ CoN ₂ O ₄	C ₅₄ H ₆₂ CoN ₂ O ₄	C ₅₄ H ₆₂ CoN ₂ O ₄	C ₅₄ H ₆₂ CoN ₂ O ₄ ·4(C ₇ H ₈)
F_w	861.99	861.99	861.99	1230.52
Cryst size, mm	0.30 × 0.26 × 0.16	0.30 × 0.26 × 0.16	0.30 × 0.26 × 0.16	0.50 × 0.34 × 0.24
Cryst sys	Triclinic	Triclinic	Triclinic	Monoclinic
Space group	$P\bar{1}$	$P\bar{1}$	$P\bar{1}$	$P2_1/n$
a , Å	10.6748(4)	10.7956(11)	9.8997(9)	16.5308(6)
b , Å	11.9906(5)	12.0991(13)	10.8120(10)	11.7257(4)
c , Å	19.6875(8)	19.834(2)	12.1278(11)	18.9821(7)
α , deg	101.316(2)	102.162(6)	104.002(5)	90
β , deg	101.9532(17)	101.446(5)	102.270(5)	107.445(2)
γ , deg	103.7626(17)	104.036(5)	101.408(5)	90
V , Å ³	2313.24(16)	2370.3(4)	1187.49(19)	3510.2(2)
Z	2	2	1	2
ρ_{calcd} , g cm ⁻³	1.238	1.208	1.205	1.164
Reflns collected/ $2\theta_{\text{max}}$, deg	75 386/56.1	75 041/55.32	56 490/56.18	12 5055/56.0
Unique reflns/ $I > 2\sigma(I)$	11 179/9566	10 996/6741	5742/4688	7474
No. of param/restraints	550/0	832/900	441/93	476/225
λ , Å/ $\mu(\text{K}\alpha)$, mm ⁻¹	0.71073/0.418	0.71073/0.408	0.71073/0.407	0.71073/0.295
R_1 [$I > 2\sigma(I)$]	0.0348	0.0422	0.0354	0.0394
wR_2 /goodness of fit	0.0921/1.042	0.1315/1.026	0.0917/1.033	0.0998
Residual density, e Å ⁻³	+0.480/−0.368	+0.340/−0.284	+0.338/−0.279	+0.487/−0.367



disorder affecting the whole ligand moieties. Two alternative orientations of the pyridyl ligand featuring inverted orientations of the central C=C double bond were refined resulting in site occupancies of 85.4(3) and 14.6(3)% of the 50 involved atoms (for a graphical representation of the disorder see ESI†). Furthermore, one of the four ^tBu groups was disordered. Here, also two different orientations were refined giving site occupancies of 52(1) and 48(1)% for the atoms C22–C24 and C22A–C24A, respectively.

The situation changed at temperatures above 295 K. At 305 K the complex molecule was now located on a crystallographic inversion center and exhibited crystallographically imposed C_i symmetry. As in the 295 K structure the pyridyl ligands were subjected to disorder with different orientations of the central C=C double bond and were refined resulting in site occupancies of 83.6(6) and 16.4(6)% of the involved atoms. Furthermore, one of the crystallographically independent ^tBu groups was disordered. Here, again two different orientations were refined giving site occupancies of 69(2) and 31(2)% for the atoms C8–C10 and C8A–C10A, respectively. All three crystal structures of *trans*-6 point to a $ls\text{-Co}^{\text{III}}(\text{Cat})(\text{SQ})$ electronic configuration (*vide infra*). However, owing to C_i symmetry at 305 K one cannot distinguish between a mixed-valent delocalized $ls\text{-Co}^{\text{III}}(\text{Cat})(\text{SQ}) \leftrightarrow ls\text{-Co}^{\text{III}}(\text{SQ})(\text{Cat})$ electronic structure and a positional disorder in the localized $ls\text{-Co}^{\text{III}}(\text{Cat})(\text{SQ})$ form.^{14,20} The observation of a crystallographic inversion center at higher temperatures may be due to increasing thermal vibration of atoms accompanied by the incipient valence tautomeric transition as confirmed by magnetic measurements.

Molecules of *cis*-6 at 100 K are located on a crystallographic inversion center and exhibit C_i symmetry. The compound crystallized with four molecules of toluene per formula unit. One of the two independent toluene molecules was disordered. Two alternative orientations were refined resulting in site occupancies of 61(1) and 39(1)% for the atoms C201–C207 and C211–C217. SAME and SIMU restraints were applied in the refinement of the disordered toluene.

Results and discussion

Syntheses and crystal structures

The neutral complexes *trans*-6 and *cis*-6 were synthesized according to a common procedure for VT cobalt dioxolenes.¹ Slow precipitation from toluene solutions afforded crystals suitable for X-ray structure determination.²⁹ At 120 K *trans*-6 reveals a distorted octahedral geometry featuring two equatorial bidentate *o*-dioxolene and two axial monodentate *trans*-4-styryl ligands (Fig. 1). Short Co–O (1.854(1)–1.916(1) Å) and Co–N (1.938(1) and 1.945(1) Å) distances are characteristic for a low-spin (*ls*) cobalt(III) ion. Intraligand C–O and (O)C–C(O) bond lengths, generally diagnostic of the oxidation level of *o*-dioxolenes,³⁰ indicate the presence of a catecholate dianion (Cat^{2-}) and a semi-quinone monoanion π -radical (SQ^-). The SQ state for one of the ligands is further confirmed by quinoid-type distortion with alternating long-short bonds. Thus, the ligand mixed valency is localized in the solid state at low temperatures.

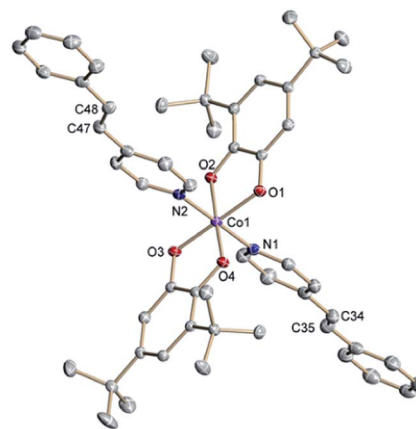


Fig. 1 Molecular structure of *trans*-6 determined at 120 K. Thermal ellipsoids are drawn at 50% probability. Hydrogen atoms are omitted for clarity.

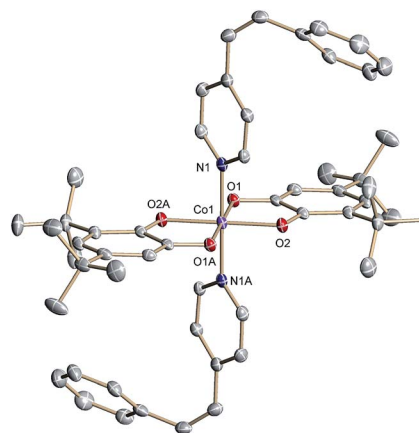


Fig. 2 Molecular structure of *cis*-6 determined at 100 K. Thermal ellipsoids are drawn at 50% probability. Hydrogen atoms are omitted for clarity.

At $T = 305$ K all cobalt–ligand bonds remain short, but the quinoid-type distortion is observed in both dioxolenes.

The structurally related *cis*-6 features two axial *cis*-4-styryl ligands (Fig. 2). Due to steric factors the pyridyl and phenyl rings of *cis*-4-styryl cannot be coplanar. Thus, the two rings form a dihedral angle of 50.1° confining a twisted ethylene bridge. Similar twisted geometry has been observed previously.^{31,32} Short Co–N (1.940(1)) and Co–O (1.885(1) and 1.878(1) Å) distances point to a $ls\text{-Co}^{\text{III}}$ center at 100 K. Similar to *trans*-6 at 305 K, intraligand bonds of both *o*-dioxolenes in *cis*-6 are equally subjected to quinoid type distortion corroborating $\text{Cat}^{2-}/\text{SQ}^-$ ligand mixed valency.

Magnetic properties in solid state

The $ls\text{-Co}^{\text{III}}(\text{Cat})(\text{SQ})$ ground state for *trans*-6 is corroborated by magnetic susceptibility measurements on a microcrystalline sample revealing an effective magnetic moment $\mu_{\text{eff}} = 1.79\mu_{\text{B}}$ invariant in the temperature range 8–250 K (see ESI†). The data could be fitted for a spin doublet $S = 1/2$ system to afford



$g = 2.064$ and a Weiss constant $\theta = -0.15$ K. Hence, based on both, bond length analysis and magnetic measurements, the electronic structure of solid *trans*-6 below 250 K is unambiguously assigned as $[\text{ls-Co}^{\text{III}}(\text{Cat})(\text{SQ})(\text{trans-4-stypy})_2]$ (*trans*-6^{LS}). At temperatures above 250 K magnetic moment gradually increased to $4.00\mu_{\text{B}}$ at 400 K revealing a thermally induced *trans*-6^{LS} \rightarrow $[\text{hs-Co}^{\text{II}}(\text{SQ})_2(\text{trans-4-stypy})_2]$ (*trans*-6^{HS}; hs = high-spin) transition. The data were fitted with the van't Hoff equation (see ESI†); with the high-temperature limit of magnetic moment fixed at $5.0\mu_{\text{B}}$ as a common value for $\text{hs-Co}^{\text{II}}(\text{SQ})_2$ isomers,¹³ our best fit provides an enthalpy change $\Delta H = 41(1)$ kJ mol⁻¹ and an entropy change $\Delta S = 104(3)$ J mol⁻¹ K⁻¹.³³

Similar to *trans*-6, magnetic data for solid *cis*-6 below 250 K were fitted for an $S = 1/2$ spin system with $g = 2.073$ and $\theta = -0.62$ K (see ESI†); and the electronic structure was assigned as $[\text{ls-Co}^{\text{III}}(\text{Cat})(\text{SQ})(\text{cis-4-stypy})_2]$ (*cis*-6^{LS}). The thermal transition *cis*-6^{LS} \rightarrow $[\text{hs-Co}^{\text{II}}(\text{SQ})_2(\text{cis-4-stypy})_2]$ (*cis*-6^{HS}), indicated by the increase in μ_{eff} at higher temperatures, was fitted to yield $\Delta H = 52(2)$ kJ mol⁻¹ and $\Delta S = 131(3)$ J mol⁻¹ K⁻¹ (see ESI†). The thermodynamic parameters obtained for both *trans*-6 and *cis*-6 in solid state are in agreement with typical thermodynamic parameters for thermally induced VT transitions.³⁴ The evolution of μ_{eff} with temperature was fully reversible without detectable hysteresis in both cases. Transition temperatures $T_{1/2}$ in solid state were estimated at 394 and 397 K for *trans*-6 and *cis*-6, respectively.

Electrochemistry

Cyclic voltammograms obtained for a CH_2Cl_2 solution of *trans*-6 at RT display one oxidation wave with a half-wave potential $E_{1/2} = -0.33$ V and two reduction events at $E_{1/2} = -0.67$ and -1.12 V versus $\text{Fc}^{+/0}$ (see ESI†). The ratio between normalized oxidative and reductive peak currents for all three waves are near unity pointing to reversible processes. However, the peak separations ΔE for reduction events significantly exceed the ideal value of 58 mV expected for a diffusion-controlled reversible one-electron transfer. Very similar cyclic voltammograms measured for *cis*-6 show one oxidation at $E_{1/2} = -0.29$ V and two reductions at $E_{1/2} = -0.69$ and -1.11 V (see ESI†). All observed redox events were assigned to the redox-active bis(dioxolene)cobalt core. Yet, a detailed assignment is difficult due to partial dissociation of the complexes in solution (*vide infra*).

Magnetic properties in solution

The effective magnetic moment of *trans*-6 in solution determined by the Evans NMR method²⁶ remained nearly constant at $1.7\mu_{\text{B}}$ below 215 K, which is in agreement with a pure $\text{ls-Co}^{\text{III}}(\text{Cat})(\text{SQ})$ state. With rising temperature, μ_{eff} gradually increased reaching $4.91(5)\mu_{\text{B}}$ at 353 K (Fig. 3). These data were fitted using the van't Hoff equation to yield $\Delta H = 43(5)$ kJ mol⁻¹, $\Delta S = 144(16)$ J mol⁻¹ K⁻¹ and the high-temperature limit of magnetic moment of $5.1(1)\mu_{\text{B}}$ that is characteristic for a pure $\text{hs-Co}^{\text{II}}(\text{SQ})_2$ state. The transition temperature $T_{1/2}$ was estimated at 299 K. At RT this solution contains 44% of $\text{hs-Co}^{\text{II}}(\text{SQ})_2$ and 56% of $\text{ls-Co}^{\text{III}}(\text{Cat})(\text{SQ})$ species as estimated from RT magnetic moment of $3.59(6)\mu_{\text{B}}$.

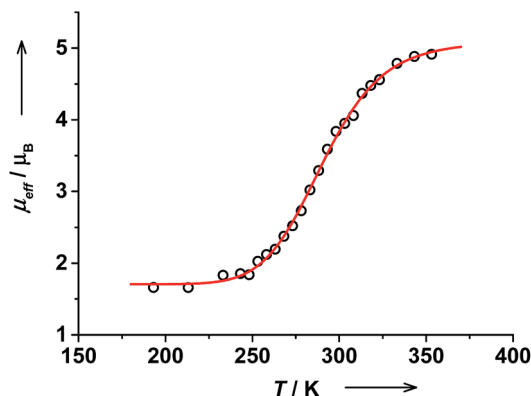


Fig. 3 Temperature dependent effective magnetic moment of *trans*-6 dissolved in toluene determined by the Evans method (toluene/[D₈] toluene/TMS = 10 : 2 : 1). Van't Hoff fit parameters: $\Delta H = 43(5)$ kJ mol⁻¹, $\Delta S = 144(16)$ J mol⁻¹ K⁻¹, low- and high-temperature magnetic moments: $\mu_{\text{eff}}(\text{LT}) = 1.69(3)\mu_{\text{B}}$ and $\mu_{\text{eff}}(\text{HT}) = 5.1(1)\mu_{\text{B}}$. Estimated transition temperature: $T_{1/2} = 299$ K.

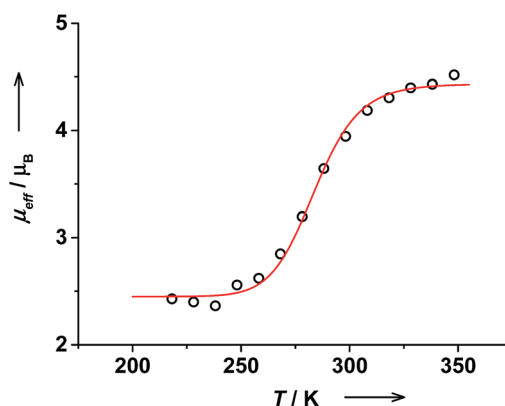


Fig. 4 Temperature dependent effective magnetic moment of *cis*-6 dissolved in toluene determined by the Evans method (toluene/[D₈] toluene/TMS = 10 : 2 : 1). Van't Hoff fit parameters: $\Delta H = 67(9)$ kJ mol⁻¹, $\Delta S = 232(33)$ J mol⁻¹ K⁻¹, low- and high-temperature magnetic moments: $\mu_{\text{eff}}(\text{LT}) = 2.45(3)\mu_{\text{B}}$ and $\mu_{\text{eff}}(\text{HT}) = 4.44(3)\mu_{\text{B}}$. Estimated transition temperature: $T_{1/2} = 287$ K.

Magnetic moment of *cis*-6 in solution changes gradually from $2.42(6)\mu_{\text{B}}$ at 218 K to $4.52(6)\mu_{\text{B}}$ at 348 K (Fig. 4). The data was fitted to give $\Delta H = 67(9)$ kJ mol⁻¹ and $\Delta S = 232(33)$ J mol⁻¹ K⁻¹. The high temperature limit for magnetic moment is $4.44(3)\mu_{\text{B}}$ that is within the range of typical values for a pure $\text{hs-Co}^{\text{II}}(\text{SQ})_2$ state.³⁵ However, the low temperature limit of $2.45(3)\mu_{\text{B}}$ is higher than expected for a pure $\text{ls-Co}^{\text{III}}(\text{Cat})(\text{SQ})$ state. This might be due to the presence of some paramagnetic impurities in solution of *cis*-6.²⁰ The transition temperature $T_{1/2}$ was estimated at 287 K. Note, that the $T_{1/2}$ value for *cis*-6 is slightly lower than that for *trans*-6 in solution (Table 2).

Electronic absorption spectra in solution

The RT electronic absorption spectrum of *trans*-6 dissolved in toluene is dominated by a strong band at 307 nm ($\epsilon = 6.1 \times 10^4$ M⁻¹ cm⁻¹) arising from $\pi \rightarrow \pi^*$ transitions of *trans*-4-stypy,

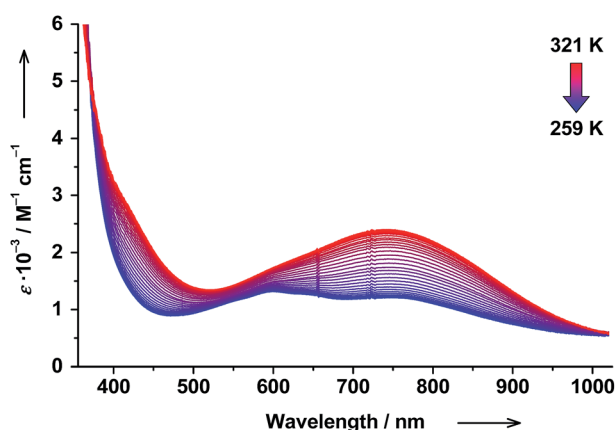
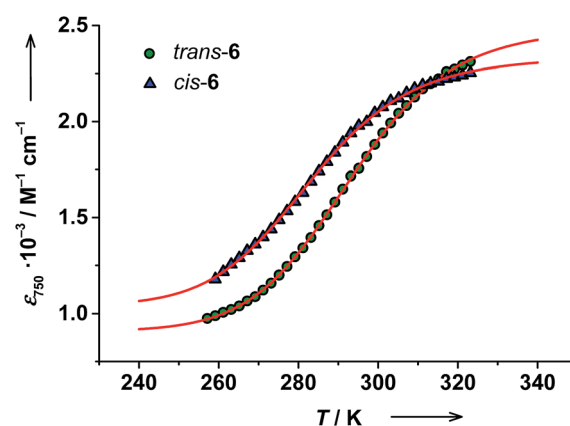


Table 2 Thermodynamic parameters determined for thermally induced transitions in *trans*-6 and *cis*-6 and estimated transition temperature $T_{1/2}$

	<i>trans</i> -6			<i>cis</i> -6		
	ΔH , kJ mol ⁻¹	ΔS , J mol ⁻¹ K ⁻¹	$T_{1/2}$, K	ΔH , kJ mol ⁻¹	ΔS , J mol ⁻¹ K ⁻¹	$T_{1/2}$, K
Solid state (SQUID)	41(1)	104(3)	394	52(2)	131(3)	397
Solution (Evans NMR)	43(5)	144(16)	299	67(9)	232(33)	287
Solution (UV-vis)	56(1)	190(5)	295	52(3)	184(11)	283
Solution (UV-vis, excess 4-stypy)	39(2)	108(9)	361	37(2)	110(7)	336

which overlap with intraligand dioxolene bands (see ESI†).^{36,37} A relatively weak broad band at 750 nm ($\epsilon = 1.8 \times 10^3 \text{ M}^{-1} \text{ cm}^{-1}$) with a shoulder at ~ 600 nm are characteristic CT transitions in VT cobalt dioxolenes.² The broad band at ~ 2650 nm, blighted by solvent overtones in the short-wavelength infrared (SWIR) region, was assigned as an intervalence ligand-to-ligand charge transfer (IVLLCT) transition, which is a spectral fingerprint of mixed-valent $\text{Is-Co}^{\text{III}}(\text{Cat})(\text{SQ})$ species (Fig. 7).³⁵ The half width $\Delta\nu_{\text{exp}}$ of this band was estimated at 860 cm^{-1} . This value is smaller than the half width calculated using the Hush equation $\Delta\nu_{\text{calcd}} = (2310 \times \nu_{\text{max}})^{1/2} = 2981 \text{ cm}^{-1}$.³⁸ Consequently, *trans*-6^{LS} behaves as a class-III fully delocalized ligand mixed-valent system in solution.

At 320 K the solution of *trans*-6 appeared green colored and the 600 nm absorption was nearly buried beneath the broad 750 nm band. Upon cooling to 259 K, the solution turned bluish-green, the 750 nm band decreased in intensity, and the absorption at 600 nm became more prominent (Fig. 5), which indicates a $\text{hs-Co}^{\text{II}}(\text{SQ})_2 \rightarrow \text{Is-Co}^{\text{III}}(\text{Cat})(\text{SQ})$ transition.²⁰ Since the available region of our spectrophotometer for variable-temperature measurements is limited to 1020 nm, the spectral evolution in the SWIR region could not be recorded. The temperature dependence of the 750 nm band was fitted according to the van't Hoff equation to yield $\Delta H = 56(1) \text{ kJ mol}^{-1}$ and $\Delta S = 190(5) \text{ J mol}^{-1} \text{ K}^{-1}$ (Fig. 6). Consequently, the estimated $T_{1/2}$ value for *trans*-6 is 295 K that is in very good agreement with the value determined by NMR spectroscopy (299 K).

**Fig. 5** Temperature-dependent electronic absorption spectra of *trans*-6 dissolved in toluene.**Fig. 6** Temperature dependence of the 750 nm absorption band of *trans*-6 and *cis*-6 dissolved in toluene. van't Hoff fit parameters for *trans*-6: $\Delta H = 56(1) \text{ kJ mol}^{-1}$, $\Delta S = 190(5) \text{ J mol}^{-1} \text{ K}^{-1}$; low- and high-temperature molar extinction coefficients: $\epsilon(\text{LT}) = 0.908(3) \times 10^3 \text{ M}^{-1} \text{ cm}^{-1}$ and $\epsilon(\text{HT}) = 2.490(4) \times 10^3 \text{ M}^{-1} \text{ cm}^{-1}$, estimated transition temperature $T_{1/2} = 295 \text{ K}$. Fit parameters for *cis*-6: $\Delta H = 52(3) \text{ kJ mol}^{-1}$, $\Delta S = 184(11) \text{ J mol}^{-1} \text{ K}^{-1}$; low- and high-temperature molar extinction coefficients: $\epsilon(\text{LT}) = 1.041(9) \times 10^3 \text{ M}^{-1} \text{ cm}^{-1}$ and $\epsilon(\text{HT}) = 2.337(5) \times 10^3 \text{ M}^{-1} \text{ cm}^{-1}$, estimated transition temperature $T_{1/2} = 283 \text{ K}$.

Similar to *trans*-6, a strong band at 306 nm ($\epsilon = 4.2 \times 10^4 \text{ M}^{-1} \text{ cm}^{-1}$) caused by *cis*-4-stypy and dioxolene intraligand transitions was observed for *cis*-6 solution at RT (see ESI†). As compared to *trans*-6, the shoulder at ~ 600 nm is less developed and the IVLLCT transition at ~ 2650 nm is weaker for *cis*-6 (see ESI†). These two features indicate that at RT the $\text{Is-Co}^{\text{III}}(\text{Cat})(\text{SQ})$ fraction in *cis*-6 solution is lower than in *trans*-6 solution. Thus, the VT equilibrium is more shifted toward the $\text{hs-Co}^{\text{II}}(\text{SQ})_2$ species in case of *cis*-6, which is very likely due to weaker coordination of *cis*-4-stypy (*vide infra*).

Similar to *trans*-complex, a color change was observed upon cooling a *cis*-6 solution. The temperature dependence of absorption at 750 nm was fitted to give $\Delta H = 52(3) \text{ kJ mol}^{-1}$ and $\Delta S = 184(11) \text{ J mol}^{-1} \text{ K}^{-1}$. The estimated $T_{1/2}$ value of 283 K is in very good agreement with the value obtained from the Evans method (287 K) (Fig. 6). Again note, that $T_{1/2}$ values for *cis*-6 are slightly lower than those of *trans*-6 in solution (Table 2).

Titration with 4-stypy ligands

The thermodynamic parameters obtained for both *trans*-6 and *cis*-6 in solution are larger than those in the solid state and



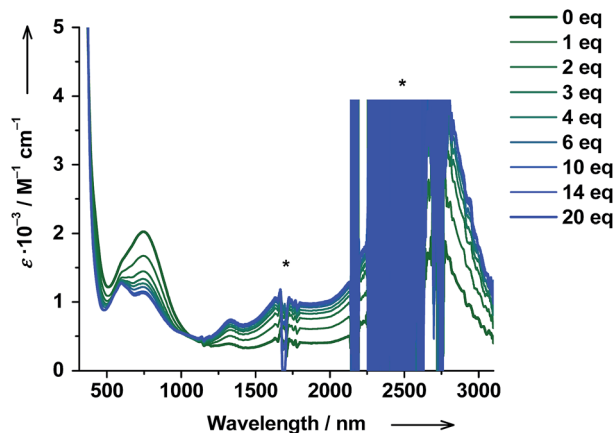


Fig. 7 Changes in absorption spectrum of *trans*-6 dissolved in toluene upon titration with *trans*-4-stypy at RT. Signals marked with asterisk (*) are due to solvent or change of detector.

clearly exceed typical values for a thermally induced VT transition, which points to partial dissociation.²⁰ The presence of a five-coordinate $\text{hs-Co}^{\text{II}}(\text{SQ})_2$ species *trans*-5 (Scheme 1) was verified by titrating a solution of *trans*-6 with *trans*-4-stypy ligand at RT. Upon addition of the ligand, the green colored solution became bluish-green, the 750 nm band decreased and absorption at 600 nm became more developed (Fig. 7). These changes closely resemble those in the variable-temperature experiments (*vide supra*) and point to a $\text{hs-Co}^{\text{II}}(\text{SQ})_2 \rightarrow \text{ls-Co}^{\text{III}}(\text{Cat})(\text{SQ})$ transition. The formation of $\text{ls-Co}^{\text{III}}(\text{Cat})(\text{SQ})$ species upon titration is further corroborated by the growing IVLLCT band at ~ 2650 nm. An isosbestic point was observed at 1060 nm. Very similar color and spectral changes were observed upon addition of *cis*-4-stypy ligand to a solution of *cis*-6 (see ESI†). Thus, the solution of *cis*-6 contains some five-coordinate *cis*-5 species.

Magnetic properties of *trans*-6 in solution changed on titration as well: the RT magnetic moment decreased gradually from $3.81(6)\mu_{\text{B}}$ (prior to *trans*-4-stypy addition) to $2.84(7)\mu_{\text{B}}$ after addition of *trans*-4-stypy (10 eq.). This is in agreement with the suggested $\text{hs-Co}^{\text{II}}(\text{SQ})_2 \rightarrow \text{ls-Co}^{\text{III}}(\text{Cat})(\text{SQ})$ switching. Similarly to *trans*-6, a decrease in μ_{eff} from $4.1(1)$ to $3.1(1)\mu_{\text{B}}$ was observed upon addition of *cis*-4-stypy (16 eq.) to a solution of *cis*-6 (see ESI†). Thus, the VT states in both *trans*- and *cis*-complexes can be switched at RT *via* addition of corresponding pyridine ligands, as we previously documented in Coordination-Induced Valence Tautomerism (CIVT) effect.²⁰

In order to obtain thermodynamic parameters for pure VT transitions between the $\text{ls-Co}^{\text{III}}(\text{Cat})(\text{SQ})$ and $\text{hs-Co}^{\text{II}}(\text{SQ})_2$ redox isomers, we recorded variable-temperature electronic spectra on solutions of *trans*-6 and *cis*-6 containing an excess of respective 4-stypy ligand. Thus, the dissociation and formation of five-coordinate species in these solutions must be suppressed. The corresponding van't Hoff fits provided $\Delta H = 39(2)$ kJ mol^{-1} and $\Delta S = 108(9)$ $\text{J mol}^{-1} \text{K}^{-1}$ for *trans*-6 and $\Delta H = 37(2)$ kJ mol^{-1} and $\Delta S = 110(7)$ $\text{J mol}^{-1} \text{K}^{-1}$ for *cis*-6 (see ESI†). Note, that these values are smaller than those obtained on solutions without excess of 4-stypy ligands and now they are in

agreement with typical values reported for VT isomers in solution.³⁵

The evolution of the electronic spectrum of *trans*-6 and the decrease of magnetic moment on titration were both fitted using a non-linear regression approach (see ESI†).³⁹ The intensity of the 750 nm absorption band as a function of *trans*-4-stypy concentration (Fig. 8) was fitted to yield an association constant $K_{\text{a}} = 4(1) \times 10^3 \text{ L mol}^{-1}$ (eqn (1)). In excellent agreement with this value, a similar fitting for magnetic moment gave $K_{\text{a}} = 6(2) \times 10^3 \text{ L mol}^{-1}$ (Fig. 9). Given the values of K_{a} , the toluene solution of the complex must contain $\sim 45\%$ of the five-coordinate *trans*-5 and $\sim 55\%$ of the six-coordinate *trans*-6 at given concentrations at RT.

Similarly, the changes of electronic spectrum and magnetic moment of *cis*-6 upon addition of *cis*-4-stypy gave K_{a} values of $1.1(3) \times 10^3$ and $0.3(1) \times 10^3 \text{ L mol}^{-1}$, respectively (see ESI†). Although there is some discrepancy in the values obtained by

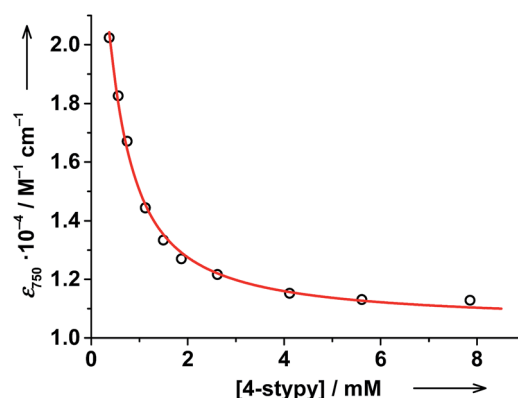


Fig. 8 The evolution of the 750 nm absorption band of *trans*-6 dissolved in toluene upon titration with *trans*-4-stypy at RT. Non-linear regression fit parameters: $\epsilon(\text{trans-6} \rightleftharpoons \{\text{trans-6}^{\text{HS}} \leftrightarrow \text{trans-6}^{\text{LS}}\}) = 1.05(2) \times 10^3 \text{ M}^{-1} \text{ cm}^{-1}$, $\epsilon(\text{trans-5}) = 2.9(1) \times 10^3 \text{ M}^{-1} \text{ cm}^{-1}$, $K_{\text{a}} = 4(1) \times 10^3 \text{ L mol}^{-1}$.

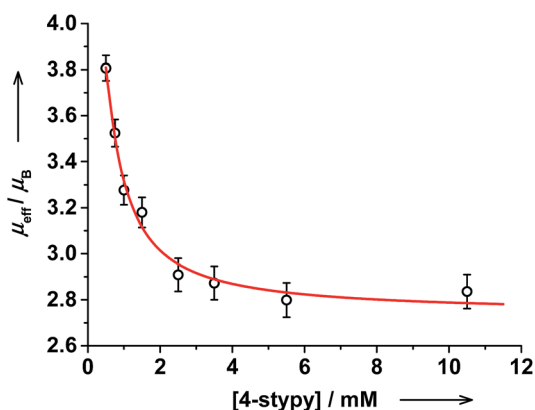
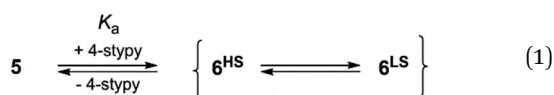


Fig. 9 The evolution of the effective magnetic moment of *trans*-6 dissolved in toluene upon titration with *trans*-4-stypy at RT determined by the Evans method (toluene/[D₈]toluene/TMS = 10 : 2 : 1). Non-linear regression fit parameters: $\mu_{\text{eff}}(\text{trans-6} \rightleftharpoons \{\text{trans-6}^{\text{HS}} \leftrightarrow \text{trans-6}^{\text{LS}}\}) = 2.51(5)\mu_{\text{B}}$, $\mu_{\text{eff}}(\text{trans-5}) = 4.7(2)\mu_{\text{B}}$, and $K_{\text{a}} = 6(2) \times 10^3 \text{ L mol}^{-1}$.



two methods, it is more important that the K_a values for *cis*-6 are significantly smaller than those for *trans*-6. Thus, *cis*-4-styryl is a weaker ligand than *trans*-4-styryl. This is corroborated by X-ray crystallography, showing that *trans*-4-styryl ligands in *trans*-6 are planar thus better π -acceptors, than non-planar *cis*-4-styryl ligands in *cis*-6.

Note, that the RT magnetic moment of dissolved *trans*-6 decreased to only $2.8\mu_B$ in the presence of a large excess of *trans*-4-styryl (20 eq.), but not to the low temperature limit of $1.7\mu_B$. This seeming inconsistency can be readily resolved by considering that the parent *trans*-6 exists as a mixture of VT isomers *trans*-6^{LS} \leftrightarrow *trans*-6^{HS} at RT in solution (eqn (1)). Thus, at low temperatures only *trans*-6^{LS} is present in solution in agreement with the observed magnetic moment of $1.7\mu_B$. At RT 45% of *trans*-6 dissociates to form *trans*-5 (*vide supra*). In the presence of a large excess of *trans*-4-styryl the dissociation is suppressed leaving a mixture of *trans*-6^{LS} and *trans*-6^{HS} at RT. The estimations from magnetic data yield 78% of *trans*-6^{LS} and 22% of *trans*-6^{HS} present in this solution at RT. The same applies to *cis*-6: in the presence of a large excess of *cis*-4-styryl the equilibrium in solution at RT is virtually shifted to six-coordinate species *cis*-6^{HS} and *cis*-6^{LS} (eqn (1)).



Photochemistry

Solutions of *trans*-6 and *cis*-6 differ in transition temperatures $T_{1/2}$ and association constants K_a . Consequently, the amount of $\text{ls-Co}^{\text{III}}(\text{Cat})(\text{SQ})$ and $\text{hs-Co}^{\text{II}}(\text{SQ})_2$ species in the two solutions is different. Thus, *trans* \leftrightarrow *cis* photoisomerization of 4-styryl ligands offers the opportunity to induce a shift in VT equilibrium and to switch magnetic properties at RT.

When *trans*-6 solution was irradiated at $\lambda = 320$ nm, the absorption band at 307 nm decreased in intensity confirming *trans*

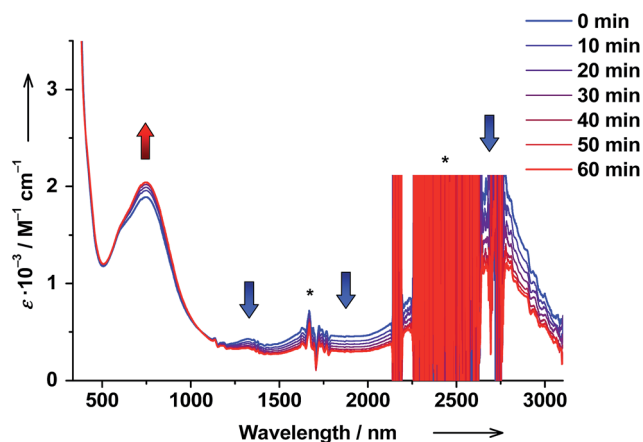


Fig. 10 Changes in absorption spectrum of *trans*-6 dissolved in toluene upon UV irradiation at RT ($c = 3.7 \times 10^{-4}$ M, $\lambda = 320 \pm 8$ nm, 1000 W Xe lamp). Signals marked with asterisk (*) are due to solvent or change of detector.

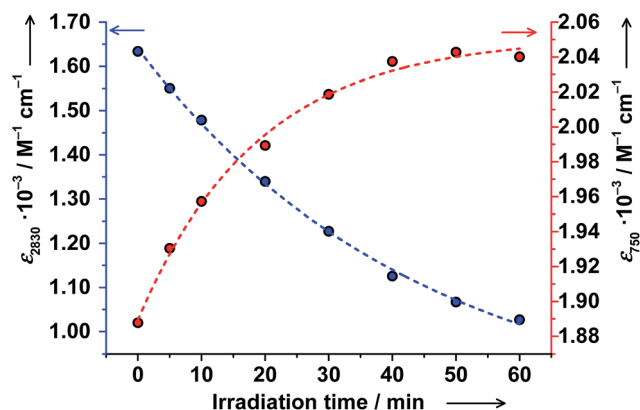


Fig. 11 Changes in absorption at 750 and 2830 nm of *trans*-6 dissolved in toluene upon UV irradiation at RT ($c = 3.7 \times 10^{-4}$ M, $\lambda = 320 \pm 8$ nm, 1000 W Xe lamp). The dashed lines serve as guides to the eye.

\rightarrow *cis* isomerization of 4-styryl (see ESI†). Upon irradiation, the IVLLCT band at ~ 2650 nm decreased and the CT band at 750 nm increased revealing an isosbestic point at 1060 nm (Fig. 10). The photostationary state (PSS) was nearly reached within 60 min (Fig. 11). It is worth mentioning that very similar spectral changes were observed for $\text{ls-Co}^{\text{III}}(\text{Cat})(\text{SQ}) \rightarrow \text{hs-Co}^{\text{II}}(\text{SQ})_2$ transition in variable-temperature and CIVT experiments (*vide supra*). Thus, the *trans* \rightarrow *cis* photoisomerization of 4-styryl did induce a VT transition in solution at RT.

These results are strongly supported by NMR spectroscopy. Upon irradiation, the magnetic moment increased gradually from $3.53(6)$ to $4.00(6)\mu_B$ and the PSS was reached within 45 min (Fig. 12). Upon further irradiation, no changes in NMR and electronic spectra were detected verifying stability of the PSS. The amount of $\text{ls-Co}^{\text{III}}(\text{Cat})(\text{SQ})$ species decreased from 60% before irradiation to 43% after irradiation. Thus, the $\text{ls-Co}^{\text{III}}(\text{Cat})(\text{SQ}) \rightarrow \text{hs-Co}^{\text{II}}(\text{SQ})_2$ photoconversion of 28% ($(60-43)/60 \times 100$) was achieved at RT. Importantly, the electronic spectrum and magnetic moment remained unchanged upon storing the irradiated solution at RT for at least 20 hours! Thus, the photogenerated VT state reveals extraordinary

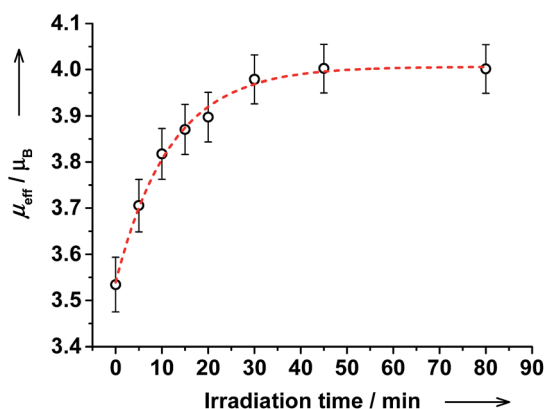


Fig. 12 The evolution of magnetic moment of *trans*-6 dissolved in toluene upon UV irradiation at RT determined by the Evans method ($c = 5.0 \times 10^{-4}$ M, toluene/ $[\text{D}_6]$ toluene/TMS = 10 : 2 : 1, $\lambda = 320 \pm 8$ nm, 1000 W Xe lamp). The dashed line serves as a guide to the eye.

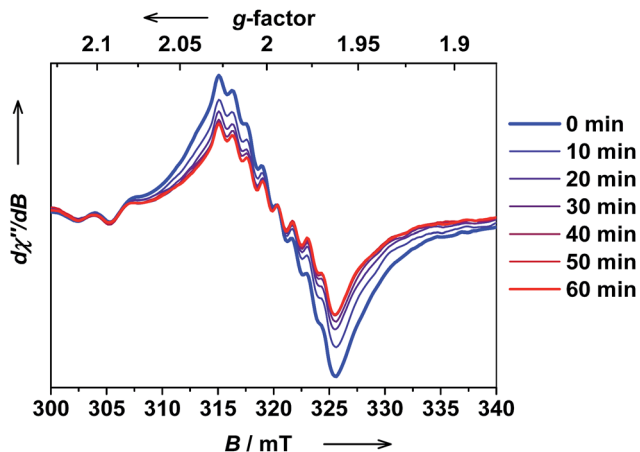


Fig. 13 The evolution of the X-band EPR spectrum of *trans*-6 dissolved in benzene upon UV irradiation at RT ($c = 1.0 \times 10^{-4}$ M, $\lambda = 323 \pm 5$ nm, 150 W Xe lamp, frequency: 8.9410 GHz, modulation: 0.7 mT, power: 20 mW). Note, that the signal is due to $\text{Is-Co}^{\text{III}}(\text{Cat})(\text{SQ})$, whereas $\text{hs-Co}^{\text{II}}(\text{SQ})_2$ species are not detected. Relatively noisy signal is due to low concentration of *trans*-6, required to speed up bulk photolysis, and consequently very small amount of EPR active $\text{Is-Co}^{\text{III}}(\text{Cat})(\text{SQ})$ species present in solution. The spectra of a more concentrated solution and at low temperatures with increased $\text{Is-Co}^{\text{III}}(\text{Cat})(\text{SQ})$ content are given in ESI†.

thermal stability at RT, as compared to common nanoseconds.⁸ This is to expect, since *cis*-4-styryl shows exceptional high thermal stability.²¹

The $\text{Is-Co}^{\text{III}}(\text{Cat})(\text{SQ}) \rightarrow \text{hs-Co}^{\text{II}}(\text{SQ})_2$ photoswitching in *trans*-6 solution was further confirmed by EPR spectroscopy. The $\text{hs-Co}^{\text{II}}(\text{SQ})_2$ isomers are usually EPR silent, whereas the $\text{Is-Co}^{\text{III}}(\text{Cat})(\text{SQ})$ state can be readily detected both at low and RT. Thus, a solution of *trans*-6 at RT shows a typical isotropic spectrum with $g_{\text{iso}} = 1.9980$ and a ^{59}Co super-hyperfine coupling constant $A_{\text{iso}} = 10.7 \times 10^{-4} \text{ cm}^{-1}$, which is synonymous with a ligand-based radical $\text{Is-Co}^{\text{III}}(\text{Cat})(\text{SQ})$.⁴⁰ Upon *in situ* irradiation at $\lambda = 323$ nm at RT, the signal of $\text{Is-Co}^{\text{III}}(\text{Cat})(\text{SQ})$ species gradually decreased, whereas no new signals appeared (Fig. 13). The PSS was reached within 60 min.

We examined the possibility to perform *trans* \rightarrow *cis* photoisomerization by low-energy excitation in visible as well.⁴¹ Whereas irradiation at $\lambda = 420$ and 750 nm did not induce desired photoreaction, irradiation at $\lambda = 600$ nm did induce *trans* \rightarrow *cis* isomerization. Unfortunately, the latter photoreaction was accompanied by some unidentified side reactions. Thus, the irradiation at $\lambda = 320$ nm is the most efficient and clear way to perform *trans* \rightarrow *cis* isomerization in *trans*-6 solution.

The reverse $\text{hs-Co}^{\text{II}}(\text{SQ})_2 \rightarrow \text{Is-Co}^{\text{III}}(\text{Cat})(\text{SQ})$ photoswitching could be accomplished as well starting from *cis*-6 complex and performing *cis* \rightarrow *trans* ligand-based photoisomerization. When *cis*-6 solution was irradiated at $\lambda = 272$ nm, the *cis* \rightarrow *trans* photoisomerization of 4-styryl could be unambiguously confirmed by increasing 306 nm band in electronic spectrum (see ESI†). Simultaneously, the 750 nm CT band decreased in intensity, a shoulder at 600 nm developed, and the LLIVCT band at ~ 2650 nm increased before the PSS was reached within 30 min

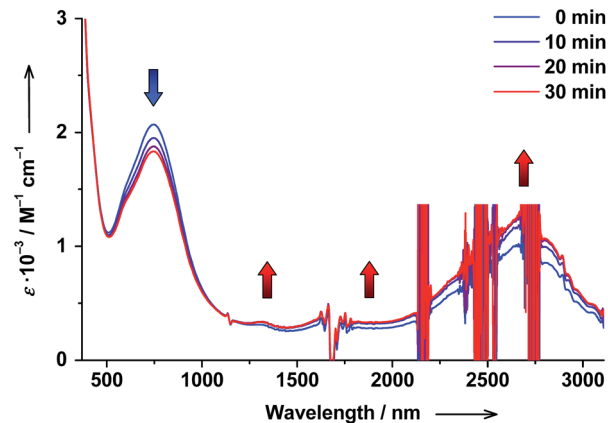


Fig. 14 Changes in absorption spectrum of *cis*-6 dissolved in benzene upon UV irradiation at RT ($c = 5.0 \times 10^{-4}$ M, $\lambda = 272 \pm 8$ nm, 1000 W Xe lamp). Signals marked with asterisk (*) are due to solvent or change of detector.

(Fig. 14). The observed spectral changes show exactly opposite trends compared to the *trans* \rightarrow *cis* photoisomerization experiment. Thus, a *cis* \rightarrow *trans* photoisomerization of 4-styryl induces $\text{hs-Co}^{\text{II}}(\text{SQ})_2 \rightarrow \text{Is-Co}^{\text{III}}(\text{Cat})(\text{SQ})$ conversion at RT.

The reverse photoswitching of VT states in *cis*-6 solution was further corroborated by the decrease of magnetic moment from 3.9(1) to 3.7(1) μ_{B} upon irradiation at $\lambda = 272$ nm (Fig. 15). After irradiation the electronic spectrum and magnetic moment remained virtually unchanged during at least 3 hours demonstrating high stability of photogenerated species.

Two mechanisms for the observed photoswitching of VT states should be considered. Upon irradiation at $\lambda = 320$ nm, *trans*-4-styryl is converted to *cis*-4-styryl (coordinated and non-coordinated). The non-planar geometry of *cis*-4-styryl renders it a weaker π -acceptor compared to the *trans*-form. Thus, the ligand field is reduced upon *trans* \rightarrow *cis* isomerization, which should stabilize the $\text{hs-Co}^{\text{II}}(\text{SQ})_2$ state in six-coordinate species 6. At the same time, *cis*-4-styryl is a weaker coordinating ligand than the *trans*-isomer,⁴² as was confirmed by differing associate

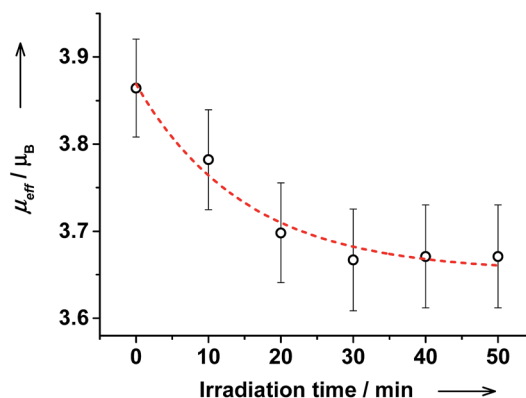


Fig. 15 The evolution of magnetic moment of *cis*-6 dissolved in toluene upon UV irradiation at RT determined by the Evans method ($c = 5.0 \times 10^{-4}$ M, toluene/ $[\text{D}_8]\text{toluene}/\text{TMS} = 10 : 2 : 1$, $\lambda = 272 \pm 8$ nm, 1000 W Xe lamp). The dashed line serves as a guide to the eye.



constants (*vide supra*). Thus, the equilibrium between five-coordinate **5** and six-coordinate **6** species is expected to shift upon *trans* → *cis* isomerization. In this case some {**6**^{LS} ↔ **6**^{HS}} species is converted to **5** increasing the hs-Co^{II}(SQ)₂ content (eqn (1)).

Similar considerations apply to reverse reaction, when *cis*-4-styppy is converted to *trans*-4-styppy by irradiating at λ = 272 nm. The observed hs-Co^{II}(SQ)₂ → ls-Co^{III}(Cat)(SQ) photoconversion may be due to increased ligand field splitting accompanying the *cis* → *trans* isomerization. Alternatively, the equilibrium between **5** and {**6**^{LS} ↔ **6**^{HS}} may be shifted toward the six-coordinate species (eqn (1)) due to stronger coordinating *trans*-4-styppy, thus leading to increased ls-Co^{III}(Cat)(SQ) content.

To gain a better mechanistic understanding, we performed an irradiation experiment on a *trans*-**6** solution containing a large excess of *trans*-4-styppy (50 eq.), in which the dissociation is virtually suppressed. Upon extended exposure to UV light the absorption spectrum did not show any detectable changes in visible and SWIR regions characteristic for VT conversion. Therefore, we concluded, that the successful photoswitching of VT states in pristine solutions of *trans*-**6** and *cis*-**6** is unlikely due to variation of the ligand field strength, but to great extent due to the light-induced shift in equilibrium between five- and six-coordinate species.

It is important to note that the photoswitching of electronic states in *trans*-**6** and *cis*-**6** solutions is of a pure molecular origin. However, the reported irradiation times (typically 30–60 min) correspond the switching of huge number of molecules (bulk photolysis), collectively detected by spectroscopic methods. Since we know how many molecules are switched from ls-Co^{III}(Cat)(SQ) to hs-Co^{II}(SQ)₂ state upon UV irradiation (appr. 10¹⁷), the effective photoswitching rate under our conditions can be estimated as 10¹⁷ molecules ÷ 3600 s = 3 × 10¹³ molecules per s.

In unison with early works by Boillot¹⁵ and recent works of Herges and Tuzek^{42,43} on bistable spin-crossover metal complexes, we coin the observed effect Ligand-Driven Light-Induced Valence Tautomerism (LD-LIVT).

Conclusions

In spite of great efforts on the development of molecular photoswitches on the base of valence tautomeric metal complexes during the last decade, the switching with light has been restricted to very low temperatures (usually below 20 K). Here, for the first time we have demonstrated light-induced switching in valence tautomeric cobalt complexes at room temperature. The driving force for the photoswitching is bidirectional *trans* ↔ *cis* photoisomerization of 4-styrylpyridine ligands deliberately integrated into bistable magnetic molecules. The photoswitching results in modulation of magnetic properties in solution at room temperature. The novel effect has been coined Ligand-Driven Light-Induced Valence Tautomerism (LD-LIVT) and proceeds at molecular level with very high effective photoswitching rates. Extensive spectroscopic studies reveal photoconversion of 28% and extraordinary thermal stability of photoinduced states at RT for hours, as compared to common

nanoseconds. Consequently, this work may open new horizons in applications of magnetic switches based on valence tautomeric metal complexes in molecular devices functioning at room temperature.

Acknowledgements

We thank the Fonds der Chemischen Industrie (Liebig Fellowship for MMK) and Deutsche Forschungsgemeinschaft (research grant KH 279/2) for financial support. Prof. Karsten Meyer (Friedrich-Alexander-University of Erlangen-Nuremberg) is acknowledged for general support. We thank Dr Andreas Scheurer and Dr Achim Zahl for assistance with NMR spectroscopy. Fabian Waidhas and Felix Ruf are acknowledged for preliminary photoexperiments with *cis*-**6**.

Notes and references

- 1 R. M. Buchanan and C. G. Pierpont, *J. Am. Chem. Soc.*, 1980, **102**, 4951–4957.
- 2 D. N. Hendrickson and C. G. Pierpont, *Top. Curr. Chem.*, 2004, **234**, 63–95.
- 3 J. Sedo, J. Saiz-Poseu, F. Busque and D. Ruiz-Molina, *Adv. Mater.*, 2013, **25**, 653–701.
- 4 V. I. Minkin, *Russ. Chem. Bull.*, 2008, **57**, 687–717.
- 5 O. Sato, J. Tao and Y.-Z. Zhang, *Angew. Chem., Int. Ed.*, 2007, **46**, 2152–2187.
- 6 A. Dei, D. Gatteschi, C. Sangregorio and L. Sorace, *Acc. Chem. Res.*, 2004, **37**, 827–835.
- 7 T. Tezgerevska, K. G. Alley and C. Boskovic, *Coord. Chem. Rev.*, 2014, **268**, 23–40.
- 8 D. M. Adams, B. L. Li, J. D. Simon and D. N. Hendrickson, *Angew. Chem., Int. Ed.*, 1995, **34**, 1481–1483.
- 9 O. Sato, S. Hayami, Z.-Z. Gu, K. Seki, R. Nakajima and A. Fujishima, *Chem. Lett.*, 2001, **30**, 874–875.
- 10 F. Varret, M. Nogues and A. Goujon, in *Magnetism: Molecules to Materials*, ed. J. S. Miller and M. Drillon, Wiley-VCH Verlag, New York, 2001, pp. 257–295.
- 11 O. Sato, A. L. Cui, R. Matsuda, J. Tao and S. Hayami, *Acc. Chem. Res.*, 2007, **40**, 361–369.
- 12 A. Beni, C. Carbonera, A. Dei, J. F. Letard, R. Righini, C. Sangregorio and L. Sorace, *J. Braz. Chem. Soc.*, 2006, **17**, 1522–1533.
- 13 R. D. Schmidt, D. A. Shultz, J. D. Martin and P. D. Boyle, *J. Am. Chem. Soc.*, 2010, **132**, 6261–6273.
- 14 R. D. Schmidt, D. A. Shultz and J. D. Martin, *Inorg. Chem.*, 2010, **49**, 3162–3168.
- 15 M.-L. Boillot, J. Zarembowitch and A. Sour, *Top. Curr. Chem.*, 2004, **234**, 261–276.
- 16 *Molecular Switches*, ed. B. L. Feringa and W. R. Browne, WILEY-VCH Verlag & Co. KGaA, Weinheim, Germany, 2011.
- 17 M. M. Paquette, R. A. Kopelman, E. Beitler and N. L. Frank, *Chem. Commun.*, 2009, 5424–5426.
- 18 M. Milek, A. Witt, C. Streb, F. W. Heinemann and M. M. Khusniyarov, *Dalton Trans.*, 2013, **42**, 5237–5241.
- 19 M. Milek, F. W. Heinemann and M. M. Khusniyarov, *Inorg. Chem.*, 2013, **52**, 11585–11592.



- 20 A. Witt, F. W. Heinemann, S. Sproules and M. M. Khusniyarov, *Chem.-Eur. J.*, 2014, **20**, 11149–11162.
- 21 J. L. R. Williams, R. E. Adel, J. M. Carlson, G. A. Reynolds, D. G. Borden and J. A. Ford, *J. Org. Chem.*, 1963, **28**, 387–390.
- 22 R. M. Buchanan, B. Fitzgerald and C. G. Pierpont, *Inorg. Chem.*, 1979, **18**, 3439–3444.
- 23 M.-C. Chiang and W. Hartung, *J. Org. Chem.*, 1945, **10**, 21–25.
- 24 E. Bill and JulX, version 1.5, *MPI for Bioinorganic Chemistry*, Muelheim/Ruhr, Germany, 2008.
- 25 F. Neese, Diploma thesis, University of Konstanz, Konstanz, Germany, 1993.
- 26 D. F. Evans, *J. Chem. Soc.*, 1959, 2003–2005.
- 27 *SADABS 2008/1*, Bruker AXS, Inc., Madison, WI, 2009.
- 28 G. Sheldrick, *Acta Crystallogr., Sect. A: Found. Crystallogr.*, 2008, **64**, 112–122.
- 29 CCDC 1015850–1015852 and 1058866 contain the supplementary crystallographic data for this paper.
- 30 C. G. Pierpont, *Coord. Chem. Rev.*, 2001, **216**, 99–125.
- 31 C. Roux, J. Zarembowitch, B. Gallois, T. Granier and R. Claude, *Inorg. Chem.*, 1994, **33**, 2273–2279.
- 32 M. L. Boillot, S. Pillet, A. Tissot, E. Rivière, N. Claiser and C. Lecomte, *Inorg. Chem.*, 2009, **48**, 4729–4736.
- 33 Variation of the high-temperature limit of the effective magnetic moment between 5.0 and 6.0 μ_B does not change the fit parameters significantly (see ESI†).
- 34 Y. Mulyana, G. Poneti, B. Moubaraki, K. S. Murray, B. F. Abrahams, L. Sorace and C. Boskovic, *Dalton Trans.*, 2010, **39**, 4757–4767.
- 35 D. M. Adams and D. N. Hendrickson, *J. Am. Chem. Soc.*, 1996, **118**, 11515–11528.
- 36 H. Rau, in *Photochromism. Molecules and Systems*, ed. H. Dürr and H. Bouas-Laurent, Elsevier, Amsterdam, 2003, pp. 64–164.
- 37 N. A. Pavlova, A. I. Poddelsky, A. S. Bogomyakov, G. K. Fukin, V. K. Cherkasov and G. A. Abakumov, *Inorg. Chem. Commun.*, 2011, **14**, 1661–1664.
- 38 N. S. Hush, in *Progress in Inorganic Chemistry*, John Wiley & Sons, Inc., 1967, pp. 391–444.
- 39 Note, that the non-linear regression fit used to obtain association constants implies only two species involved into equilibrium, whereas actually three species (5, 6^{LT} and 6^{HT}) are present in solution. However, the employed model is still valid, if the temperature is kept constant and thus the ratio between 6^{LT} and 6^{HT} remains constant too. Hence, the model describing the equilibrium between 5 and a quasi-species $\{6^{LT} \leftrightarrow 6^{HT}\}$ is correct.
- 40 D. M. Adams, L. Noodleman and D. N. Hendrickson, *Inorg. Chem.*, 1997, **36**, 3966–3984.
- 41 A. Tissot, M.-L. Boillot, S. Pillet, E. Codjovi, K. Boukheddaden and L. M. L. Daku, *J. Phys. Chem. C*, 2010, **114**, 21715–21722.
- 42 S. Thies, H. Sell, C. Schütt, C. Bornholdt, C. Näther, F. Tuczek and R. Herges, *J. Am. Chem. Soc.*, 2011, **133**, 16243–16250.
- 43 S. Venkataramani, U. Jana, M. Dommaschk, F. D. Sonnichsen, F. Tuczek and R. Herges, *Science*, 2011, **331**, 445–448.

